



Highly efficient accelerator of dense matter using laser-induced cavity pressure acceleration

J. Badziak, S. Jabłoński, T. Pisarczyk, P. Rączka, E. Krousky et al.

Citation: [Phys. Plasmas](#) **19**, 053105 (2012); doi: 10.1063/1.4714660

View online: <http://dx.doi.org/10.1063/1.4714660>

View Table of Contents: <http://pop.aip.org/resource/1/PHPAEN/v19/i5>

Published by the [American Institute of Physics](#).

Related Articles

Effect of pulse profile and chirp on a laser wakefield generation

[Phys. Plasmas](#) **19**, 053103 (2012)

Enhancement of x-rays generated by a guided laser wakefield accelerator inside capillary tubes

[Appl. Phys. Lett.](#) **100**, 191106 (2012)

2D particle-in-cell simulations of ion acceleration in laser irradiated submicron clusters including field ionization

[Phys. Plasmas](#) **19**, 043107 (2012)

Simulation of the runaway electron beam formed in a discharge in air at atmospheric pressure

[Phys. Plasmas](#) **19**, 043105 (2012)

Self consistent model for ponderomotive ion acceleration of laser irradiated two species dense target plasmas

[Phys. Plasmas](#) **19**, 043104 (2012)

Additional information on Phys. Plasmas

Journal Homepage: <http://pop.aip.org/>

Journal Information: http://pop.aip.org/about/about_the_journal

Top downloads: http://pop.aip.org/features/most_downloaded

Information for Authors: <http://pop.aip.org/authors>

ADVERTISEMENT

An advertisement for AIP Advances. The top part features the 'AIP Advances' logo in green and blue, with a series of orange circles of varying sizes to its right. Below this, the text 'Special Topic Section: PHYSICS OF CANCER' is written in white on a dark green background. At the bottom, the phrase 'Why cancer? Why physics?' is written in yellow, and a blue button with the text 'View Articles Now' is positioned on the right.

AIP Advances

Special Topic Section:
PHYSICS OF CANCER

Why cancer? Why physics? [View Articles Now](#)

Highly efficient accelerator of dense matter using laser-induced cavity pressure acceleration

J. Badziak,^{1,a)} S. Jabłoński,¹ T. Pisarczyk,¹ P. Rączka,¹ E. Krousky,² R. Liska,³ M. Kucharik,³ T. Chodukowski,¹ Z. Kalinowska,¹ P. Parys,¹ M. Rosiński,¹ S. Borodziuk,¹ and J. Ullschmied⁴

¹*Institute of Plasma Physics and Laser Microfusion, 01-497 Warsaw, Poland*

²*Institute of Physics, AS CR, 182 21 Prague 8, Czech Republic*

³*Czech Technical University, FNSPE, 160 41 Prague 6, Czech Republic*

⁴*Institute of Plasma Physics, AS CR, 182 20 Prague 8, Czech Republic*

(Received 9 January 2012; accepted 12 April 2012; published online 15 May 2012)

Acceleration of dense matter to high velocities is of high importance for high energy density physics, inertial confinement fusion, or space research. The acceleration schemes employed so far are capable of accelerating dense microprojectiles to velocities approaching 1000 km/s; however, the energetic efficiency of acceleration is low. Here, we propose and demonstrate a highly efficient scheme of acceleration of dense matter in which a projectile placed in a cavity is irradiated by a laser beam introduced into the cavity through a hole and then accelerated in a guiding channel by the pressure of a hot plasma produced in the cavity by the laser beam or by the photon pressure of the ultra-intense laser radiation trapped in the cavity. We show that the acceleration efficiency in this scheme can be much higher than that achieved so far and that sub-relativistic projectile velocities are feasible in the radiation pressure regime. © 2012 American Institute of Physics. [<http://dx.doi.org/10.1063/1.4714660>]

I. INTRODUCTION

Acceleration of projectiles of dense matter to hypervelocities has been a challenge for science and technology for a long time. Currently, this topic is of high relevance for contemporary research in the high energy-density physics (HEDP),¹ inertial confinement fusion (ICF),² nuclear physics,³ and space research.^{4,5} Various schemes of the acceleration were proposed and their ability to reach projectile parameters not attainable with the use of chemical propellants had been demonstrated. These include electromagnetic rail guns,⁶ Van de Graaf accelerators,⁴ Z-pinch machines,⁷ coaxial plasma guns,⁸ and laser-driven accelerators.^{2,9–13} Among these, only laser-driven acceleration schemes are presently capable of accelerating dense matter (usually plasma) projectiles (i.e., compact macroscopic objects of the average electron density of the order of 10^{22} cm⁻³ or higher) to velocities in the range 100–1000 km/s.^{2,9,10,14}

The most commonly used scheme of laser-driven dense projectile acceleration relies on the so called ablative acceleration (AA).^{2,9,10,14} In the AA scheme, the surface of a solid target is subject to an intense irradiation (either directly by the laser beam or indirectly via secondary radiation induced by the laser), which leads to the creation of a hot plasma that expands backward, thus accelerating the remaining denser part of the target (the projectile) in the forward direction via the “rocket effect.”² The AA scheme is the mainstay of the ICF research, where it is used to accelerate and compress DT fuel in fusion targets^{2,14} or to accelerate a microprojectile to ignite the fuel by the impact.^{9,15,16} Unfortunately, this scheme has a relatively low energetic efficiency of accelera-

tion $\eta_{\text{acc}} = E_p/E_L$, where E_p is the kinetic energy of the projectile and E_L is the energy supplied by the laser driver, which in practice is below 10%.^{2,14,16} There have been various attempts to increase the efficiency of laser-driven acceleration: using a cannonball-like fusion target (CBT),¹⁷ employing the reverse acceleration scheme (RAS),¹⁸ as well as applying double ablation (DA),^{9,19} or two-color irradiation (TCI).²⁰ However, either an increase in η_{acc} in the proposed schemes is relatively small (DA and TCI [within a factor ~ 2 (Ref. 19)] or their practical usefulness has not been demonstrated (CBT and RAS).

The AA scheme has also another limitation: the maximum attainable velocity of the projectile is limited due to the Rayleigh-Taylor (RT) instability to about 10^8 cm/s. This limit for the projectile velocity may be shifted to relativistic velocities by relying on the radiation pressure acceleration (RPA) (Refs. 11, 13, and 21–24) [also referred to as skin-layer ponderomotive acceleration – SLPA (Refs. 13, 25, and 26)]. In the RPA scheme, an ion (plasma) bunch is driven by the radiation (photon) pressure of a short (ps or sub-ps) laser pulse of high intensity ($I_L \gg 10^{18}$ W/cm²). The efficiency of these schemes may reach tens of percent^{13,21,22} in the relativistic regime. Unfortunately, at high but non-relativistic velocities, which are important for many applications (e.g., for ICF and HEDP), the acceleration efficiency in the RPA scheme is lower^{13,23} and can be comparable to that in the AA scheme.

In this paper, we propose and investigate a novel, highly efficient scheme of laser-driven acceleration of dense matter, which combines the old idea of conventional gun with the ideas of the cannonball target and radiation pressure acceleration. Apart from very high energetic efficiency, significantly higher than that achieved so far, the proposed scheme has a potential to accelerate dense projectiles to near-

^{a)}E-mail: jan.badziak@ifpilm.pl.

relativistic velocities. Hereafter, this scheme will be referred to as laser-induced cavity pressure acceleration (LICPA).

II. LASER-INDUCED CAVITY PRESSURE ACCELERATION

In the LICPA scheme (Fig. 1), a projectile placed in a cavity is irradiated by a laser beam introduced into the cavity through a hole; the projectile is then accelerated in a guiding channel (cylindrical or conical) by the pressure created in cavity by the laser-produced hot plasma expanding from the irradiated side of the projectile and from the cavity walls or by the photon (radiation) pressure of the ultra-intense laser radiation trapped in the cavity. An important part of the scheme is the guiding channel, which plays a role similar to that of a barrel in a conventional gun, allowing the accelerating forces to act for an extended period of time, as well as collimating and compressing the plasma projectile.

Depending on the laser intensity and the pulse length, different regimes of the LICPA accelerator operation can be distinguished. At relatively low laser intensities and moderately long laser pulses (say, at $I_L < 10^{17}$ W/cm² and $\tau_L > 10^{-11}$ s), we can speak about a pure hydrodynamic LICPA regime, as the dominating force driving the projectile is due to the hydrodynamic pressure of hot plasma produced and confined in the accelerator cavity. In this regime, there is an upper limit for the pulse length $\tau_L^{\max} \sim L_c/v_{pl}$, where L_c is the cavity length and v_{pl} is the velocity of overdense plasma expanding in the cavity. It means that, for e.g., $L_c \sim 0.5$ mm, we have $\tau_L^{\max} \sim 1$ ns at $I_L \sim 10^{15}$ – 10^{16} W/cm², or $\tau_L^{\max} \sim 10$ ns at $I_L \sim 10^{10}$ – 10^{11} W/cm². On the other hand, at very high laser intensities and short laser pulses of circular polarization (say, at $I_L \geq 10^{20}$ W/cm², $\tau_L \leq 10^{-11}$ s), the photon pressure LICPA regime occurs, as the acceleration of the projectile is predominantly due to the photon pressure of radiation confined in the cavity. For intermediate laser intensities (say, 10^{17} W/cm² $\leq I_L < 10^{20}$ W/cm²), we may speak about a mixed LICPA regime, as, in this case, there is a complicated interplay between hydrodynamic and photon pressure and a large amount of non-thermal hot electrons is produced.

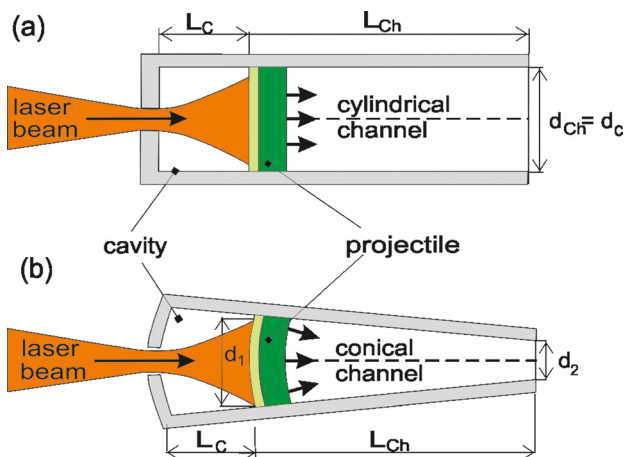


FIG. 1. Two geometries of laser-driven accelerators of dense matter using LICPA: (a) the cylindrical accelerator and (b) the conical accelerator.

In the following, the basic properties of the LICPA accelerator working in the hydrodynamic regime (Sec. III) and the photon pressure regime (Sec. IV) are discussed in detail. Preliminary results of our studies of the hydrodynamic LICPA accelerator have been presented in Ref. 27.

III. THE HYDRODYNAMIC LICPA ACCELERATOR

To understand basic properties of the hydrodynamic LICPA accelerator and to estimate its energetic efficiency, we performed a series of experiments using 1ω ($\lambda = 1.315$ μm) or 3ω ($\lambda = 0.438$ μm) beams of the kilojoule PALS laser facility,²⁸ supplemented by advanced hydrodynamic simulations. The energy of the laser pulse (of 0.3 ns duration) varied from 50 J up to 400 J and the laser intensity on the target varied from 2×10^{14} W/cm² up to 5×10^{15} W/cm². In the experiments, we measured dimensions of craters produced in the massive Al target (placed close to the accelerator guiding channel exit) by the plasma projectile produced and accelerated in the LICPA accelerator (using the replica technique). We also measured the characteristics of the plasma flux leaving the guiding channel in a close vicinity of the channel exit (by means of interferometry or shadowgraphy using the three-frame interferometric system with the 2ω PALS laser probe beam²⁹) and at a distance of 30 cm from the channel exit on the laser beam axis (by means of the time-of-flight method using ion collectors³⁰). The measurements were carried out for both cylindrical and conical LICPA accelerators of various geometrical and material characteristics: the cavity length $L_c = 0.1, 0.2,$ and 0.4 mm; the guiding channel length $L_{ch} = 0, 1, 2,$ and 3 mm; the cavity aperture $d_c = 0.3$ and 0.45 mm; the entrance cavity hole aperture $d_h = 0.15$ and 0.23 mm; the channel entrance aperture $d_1 = d_c$; the channel exit aperture $d_2 = 0.1, 0.15,$ and 0.3 mm; the foil target of planar or curved shape (section of a sphere of the radius $r_t = 2, 3,$ or 4 mm); the foil target material: CH, CD₂, and Al covered by 2.5 μm mylar or 5 μm polystyrene ablator; the foil target thickness: $l_t = 10, 20,$ and 30 μm for CH, $l_t = 25$ and 50 μm for CD₂, and $l_t = 6, 10, 20, 50,$ and 75 μm for Al ($+2.5$ μm mylar or 5 μm polystyrene); the cavity and the channel walls material: Au or Al. The results of measurements obtained for the LICPA accelerators were compared with the those obtained for the AA schemes with the same geometrical and material parameters as LICPA, but without a cavity, and the same laser beam energy and intensity on the foil target. The comparison was done for a majority of the considered configurations for both cylindrical and conical accelerators. Moreover, some results obtained with the use of LICPA accelerator were compared with those for the direct laser-target (Al massive, CH, or CD₂) interaction (the L-T scheme). To obtain credible results, more than 300 high-energy (~ 50 – 400 J) laser shots were done in three experimental campaigns. The selected results presented in this paper are representative of the large quantity of the collected data. The conclusions reached in this note are valid for all investigated LICPA and AA schemes.

The key parameter of the accelerated projectile is its kinetic energy. An effective indirect way to estimate this energy is to measure the volume of the crater produced by

the collision of the projectile with a massive target. Since the scaling laws that relate the crater volume and the projectile energy were not available in the literature, we had to resort to numerical simulations; these were done using a 2-dimensional hydrodynamic PALE code.³¹ The code employs the Arbitrary Lagrangian Eulerian (ALE) method³² to overcome the difficulties connected with distortion and tangling of the moving Lagrangian mesh. It uses compatible staggered Lagrangian scheme³³ for the Lagrangian step, several different methods for mesh smoothing, and swept area remapping³⁴ for conservative interpolation of the hydrodynamical quantities from the Lagrangian computational mesh to the smoothed one. Heat conductivity with heat flux limiting is treated by the mimetic method³⁵ with classical Spitzer-Harm heat conductivity coefficient. The laser absorption (the collisional and the resonance one) is modeled by ray tracing. The code is routinely used to simulate laser-target interactions,^{31,36} mainly for the interpretation of experiments performed at the PALS laser facility.

The hydrodynamic simulations presented in this paper are performed in two phases. In the first phase, the laser absorption is simulated together with the ablative acceleration of the projectile through the channel. This simulation is stopped in the moment (long after the end of the laser pulse) when the moving projectile reaches the end of the channel. At this point, the snapshot of computed hydrodynamic quantities is saved and then interpolated to a new initial computational mesh, providing the initial conditions for the second phase-impact simulation. The impact of the accelerated projectile into the massive Al target creates a crater in the target. By the simulated crater, we understand the region of evaporated and melted aluminum. The growth of the crater volume stops at certain time (much longer for LICPA than AA) when there is not enough energy available to melt the Al target further. This gives us the volume and shape of the simulated crater.

The replicas of the craters produced in the massive Al target by plasma projectiles are shown in Fig. 2, and quantitative results showing the dependence of the crater volume on the laser energy in the LICPA and AA schemes with different geometries are presented in Figs. 3 and 4, respectively. For all geometries and laser parameters that were used, the volumes of craters produced by the projectiles driven in the LICPA accelerators were significantly bigger than those obtained with projectiles driven by AA, by a factor of 20 for the 3ω beam (Figs. 3 and 4) and a factor of 100 and more for the 1ω beam (Fig. 4).

The craters produced by the plasma projectile driven in the LICPA accelerator were also compared with the craters created in the massive Al target by a direct laser-target interaction (the L-T scheme), as well as craters formed by the CH foil directly irradiated by the laser beam and accelerated in free space (the distance between the CH foil and the Al target $L_{\text{CH-Al}}$ was equal to the channel length L_{Ch} in the LICPA scheme). We observed that the craters produced in the L-T scheme were smaller by a factor of 20–50 than in the LICPA case. In the case of CH foil target accelerated in free space, no clear crater was produced at $L_{\text{CH-Al}} = L_{\text{Ch}}$. We also measured the craters produced by the CH target driven by LICPA but in the scheme without a guiding channel. In this case,

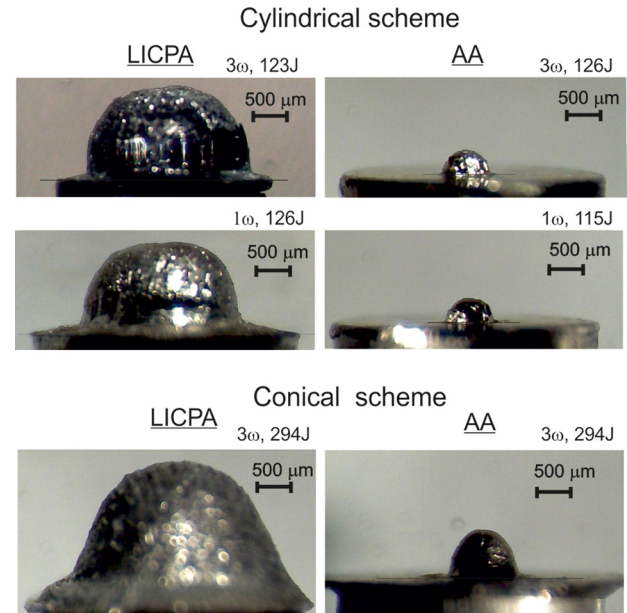


FIG. 2. Replicas of craters produced in the massive Al targets by plasma projectiles accelerated in the LICPA and AA schemes with cylindrical and conical geometry. For the cylindrical geometry, the target was $l_t = 20 \mu\text{m}$ CH foil, and $L_{\text{Ch}} = 2 \text{ mm}$, $d_c = 0.3 \text{ mm}$, $L_c = 0.1 \text{ mm}$, $d_h = 0.15 \text{ mm}$. For the conical geometry, the target was $l_t = 25 \mu\text{m}$ CD₂ foil, with $r_t = 2 \text{ mm}$, $L_{\text{Ch}} = 2 \text{ mm}$, $L_c = 0.4 \text{ mm}$, $d_1 = d_c = 0.45 \text{ mm}$, $d_2 = 0.15 \text{ mm}$, $d_h = 0.23 \text{ mm}$. All the accelerators were made of Au.

both the volumes and depths of craters produced at $L_{\text{CH-Al}} = L_{\text{Ch}} = 1, 2, \text{ or } 3 \text{ mm}$ were an order of magnitude smaller than in the case of “complete” LICPA accelerator containing the guiding channel. This measurement proves that the guiding channel really plays a key role in the LICPA accelerator and it can significantly enhance projectile parameters.

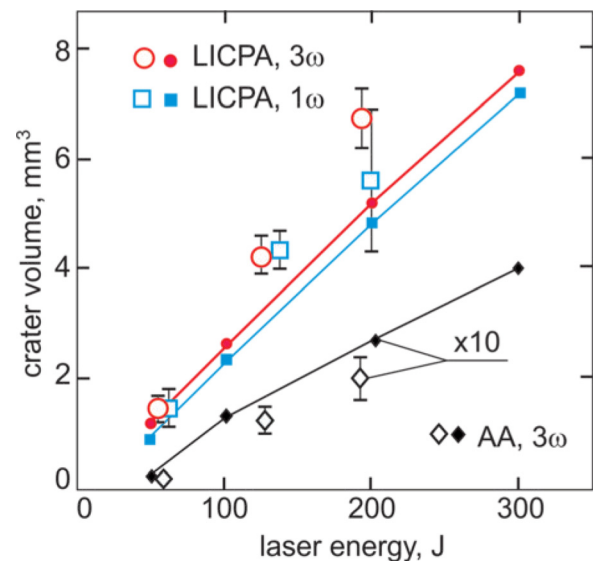


FIG. 3. The volume of craters produced by the plasma projectile in the massive Al target, as a function of laser energy, for the cylindrical LICPA and AA schemes, with the same parameters as in Fig. 2. Circles, squares, and diamonds with error bars represent experimental data, while smaller bullets connected by solid lines represent numerical hydrodynamic simulations. Note that the crater volumes for AA are magnified by the factor 10 in the figure.

In addition to experimental results, we also show in Figs. 3 and 5 the results of numerical simulations of the plasma projectile acceleration and its collision with the massive Al target. Simulations were performed for the LICPA and AA schemes in the cylindrical geometry. The volumes of the craters and their shapes predicted by the simulation match fairly well those obtained experimentally: the volumes for LICPA scheme appear to be underestimated by a factor ~ 1.3 , and for AA scheme (3ω beam), they are overestimated by a factor ~ 1.6 . It is of key importance that, in spite of a relatively small difference in the total absorption coefficient for LICPA and AA (the difference was 25%–60% for 3ω), the predicted (and measured) crater volumes for LICPA are more than an order of magnitude higher than those attained with AA. The main reason for this is the fact that in the AA scheme more than 70%–80% of the absorbed energy is converted into the energy of ablating plasma (which is lost in this scheme) and only $\sim 10\%$ or less of the absorbed energy is transformed in the kinetic energy of the projectile (remaining part of the absorbed energy goes into the projectile thermal energy). In the LICPA scheme, almost all energy of the ablated plasma is confined in the cavity, and most of this energy can be transformed in the kinetic energy of the projectile. Thus, in a well optimized LICPA scheme, the main “un-useful” part of the absorbed energy can be only the thermal energy of the projectile and the hydrodynamic efficiency of acceleration $\eta_h = E_p/E_L^{\text{abs}}$ can reach even 90%. It is also important that (as it results from our simulations) the plasma projectile accelerated in the LICPA scheme is not only faster but also much more dense (by an order of magnitude for the cylindrical scheme) and compact than in the AA scheme.

A significant enhancement of parameters of the plasma projectiles in the case of the LICPA scheme is confirmed by interferometric and ion diagnostic, as shown in Figs. 6–8. It

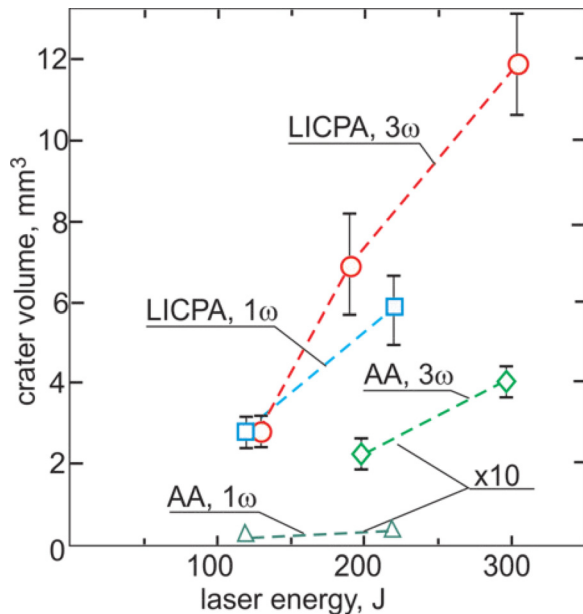


FIG. 4. The volume of craters produced by the plasma projectile in the massive Al target, as a function of laser energy, for the conical LICPA and AA schemes with the same parameters as in Fig. 2. Note that the crater volumes for AA are magnified by the factor 10 in the figure.

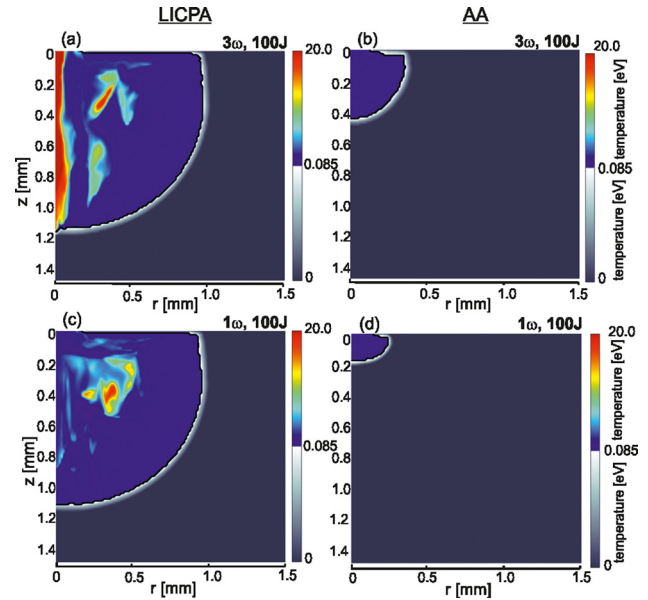


FIG. 5. Temperature distributions of the Al target in the final stage of crater formation by the impact of the plasma projectile accelerated in the LICPA or in the AA cylindrical schemes with the same parameters as in Fig. 2. The gray boundary between the blue and the dark-blue region is the boundary between the melted and the solid part of the target.

can be seen that the plasma flux leaving the LICPA accelerator is denser, faster (the average velocity of dense plasma in the channel reaches $\sim 2 \times 10^7$ cm/s), and carries much more electrons (and ions) than the plasma flux flowing out of the channel in the AA accelerator. Our calculations of the plasma outflow velocity, dN_e/dt , based on the three-frame interferometric measurements (Fig. 7), proved that the values of dN_e/dt for the plasma outflows for the LICPA scheme (both in the cylindrical and conical geometry) are higher by at least a factor of 10 than the ones for the AA scheme, even when the high-density (opacity) zone for LICPA (seen in Fig. 6) was

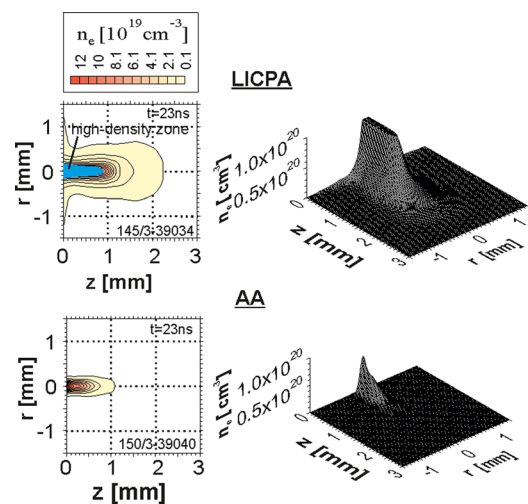


FIG. 6. The electron isodensitograms and the space profiles of electron distributions for the plasma flowing out of the channel in the LICPA and AA cylindrical schemes recorded 23 ns after the target irradiation. CD_2 target of $l_t = 25 \mu\text{m}$, $L_{\text{Ch}} = 2 \text{ mm}$, $d_c = 0.3 \text{ mm}$, $L_c = 0.2 \text{ mm}$, $d_h = 0.15 \text{ mm}$. 3ω laser beam of $E_L = 177 \text{ J}$ for LICPA and 180 J for AA. Note that the plasma driven by LICPA is faster and carries much more electrons and ions than that driven by AA.

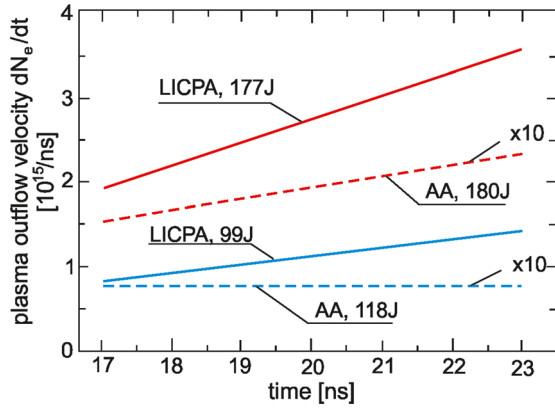


FIG. 7. Plasma outflow velocity as a function of time for the plasma flowing out of the channel in the LICPA and AA cylindrical schemes with the same parameters as in Fig. 6. Note that the outflow velocity for AA scheme is magnified by the factor 10 in the figure.

neglected in the calculations. A considerable enhancement of the ion current at the distance of 30 cm from the end of the channel is also clearly seen, as shown in Fig. 8.

Relying on the fact that experimental results and numerical predictions shown in Fig. 3 are fairly consistent, we may try to estimate the acceleration efficiency, $\eta_{\text{acc}} = E_p/E_L$, for the LICPA and AA schemes. Fig. 9 presents the acceleration efficiency in these schemes, as given by the numerical simulation using the PALE code, performed for the physical conditions identical to those assumed for the results presented in Fig. 3. The value of η_{acc} computed for LICPA and AA (3ω), corresponds to the kinetic energy E_p (E_L), which results in the crater volume V_c (E_L) in the numerical scaling laws plotted in Fig. 3. It was taken into account that the total projectile energy $E_p^{\text{tot}} = E_p + E_p^i$, where E_p^i is the internal (thermal) projectile energy computed together with E_p^{tot} and E_p . The acceleration efficiency for LICPA changes very slowly with the laser energy/intensity (the projectile energy increases almost linearly with an increase in E_L), and for both 1ω and 3ω , it

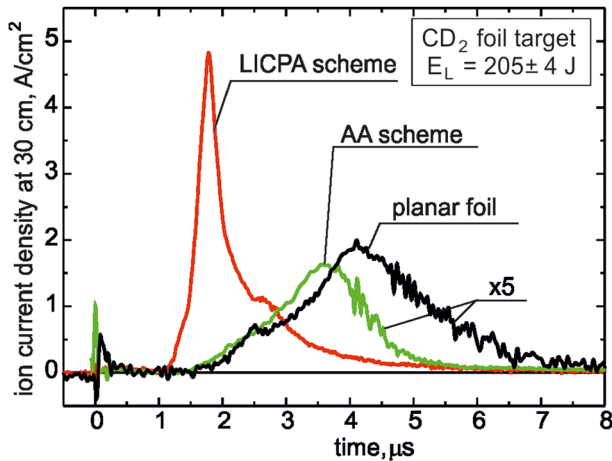


FIG. 8. The ion current density of plasma driven by the 3ω laser beam in the LICPA and AA cylindrical schemes (of parameters as in Fig. 6) as well as of the plasma produced at the direct interaction of the beam with 25- μm CD_2 planar target. Note that the ion current densities for the AA scheme and the planar foil (the L-T scheme) are magnified by the factor 5 in the figure. The ion current density is by more than a factor 10 higher and the mean ion energy is by more than a factor 4 higher for LICPA than those for AA and L-T.

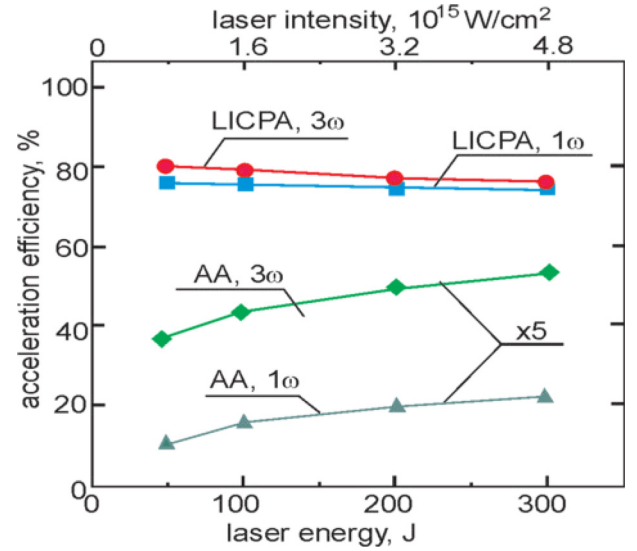


FIG. 9. The acceleration efficiency of plasma projectiles driven in the LICPA and AA cylindrical schemes (with parameters as in Fig. 3), as a function of laser energy. Note that the acceleration efficiency for the AA scheme is magnified by the factor 5 in the figure.

reaches the values in the range of 70%–80%. The efficiency for AA increases with increasing E_L and reaches 10.6% for 3ω and 4.4% for 1ω . Thus, the ratio $R_\eta = \eta_{\text{acc}}^{\text{LICPA}}/\eta_{\text{acc}}^{\text{AA}}$ of the acceleration efficiencies in the LICPA scheme and the AA scheme decreases with E_L from the value 11 to 7 for 3ω and from the value 34 to 16 for 1ω . Being very conservative, we may thus conclude that, for both the 1ω and the 3ω laser beam and for the range of laser pulse energies and intensities relevant for our experiment, the efficiency of the LICPA accelerator can reach values above 50%, i.e., values higher than in the AA scheme by a factor of at least 5 for the 3ω beam and a factor of at least 10 for the 1ω beam.

IV. THE PHOTON PRESSURE-DRIVEN LICPA ACCELERATOR

To demonstrate basic properties of the LICPA accelerator in the photon pressure regime and to compare it with the conventional RPA scheme, we will use results of 1-dimensional (1D) numerical particle-in cell (PIC) simulations as well as a simple analytic model of the accelerator, which generalizes the well known light-sail acceleration model.^{24,37}

In the simulations, we assumed that both the laser radiation in the cavity and the irradiated overdense target (projectile) are homogeneous in the directions perpendicular to the laser radiation propagation axis. The laser radiation, introduced into the cavity through a hole (see Fig. 1), is reflected from the target in the direction opposite to the laser beam, then reflected again at the inner cavity wall (with the intensity reflection coefficient R_c), at a distance L_c from the target, and redirected back towards the target. As a result, the radiation circulates in the cavity, building up the photon (radiation) pressure in the cavity that accelerates the target. To simulate the plasma projectile dynamics, we used the relativistic 1D PIC code,³⁸ which is a modified version of the well known LPIC++ code³⁹ adapted to our needs. In the simulations, a laser beam interacts with a target consisting of a

homogeneous layer of fully ionized plasma of L_T thickness and an exponential preplasma layer on the target's front side of the density gradient scale length $L_n = 0.25 \mu\text{m}$. The simulations were performed for four different ion species: H^+ , Be^{4+} , C^{6+} , and Al^{13+} of realistic ion masses m_i and densities $n_i = z n_e$ (z is the ion charge state and n_e is the electron density). The value of L_T was selected in such a way that the areal mass density $\sigma_h = \rho L_T$ was the same for each target and equal to $\sigma_h = 4 \times 10^{-4} \text{ g/cm}^2$ (it means that, e.g., for the carbon plasma, $L_T = 2 \mu\text{m}$, $n_i = 10^{23} \text{ cm}^{-3}$, and for the hydrogen plasma, $L_T = 28.6 \mu\text{m}$, $n_i = 0.84 \times 10^{23} \text{ cm}^{-3}$). However, the total areal mass density σ , which also incorporates the areal mass density of the preplasma layer, was a bit different for each kind of plasmas (L_n was the same for plasmas of different ρ), which enabled us to observe the sensitivity of the projectile parameters on σ both in the PIC simulations and the analytic model. Since one of the important possible applications of the LICPA accelerator is the ICF fast ignition, the laser beam parameters (the target parameters as well) were selected to be relevant to the ion fast ignition scenario.^{40,41} In particular, we assumed a circularly polarized laser pulse of the wavelength $\lambda = 1.06 \mu\text{m}$, the duration (FWHM) $\tau_L = 2 \text{ ps}$, and a super-Gaussian profile $I(t) = I_L \exp(-t^6/\tau_L^6)$ with $I_L = 2.5 \times 10^{21} \text{ W/cm}^2$ (which for the focal spot size of $50 \mu\text{m}$ corresponds to $100 \text{ kJ} / 50 \text{ PW}$ laser pulse). The cavity length L_c was varied in the range $40\text{--}160 \mu\text{m}$, and the cavity wall reflection coefficient was assumed, rather conservatively, $R_c = 0.64$ (1/3 of the radiation reflected from the target is lost in each cycle due to imperfectness of the wall reflectivity and an escape of the radiation through the hole).

The analytic model of the photon pressure-driven LICPA accelerator generalizes the light-sail (LS) acceleration model^{24,37} to incorporate circulation of the laser radiation in the accelerator cavity. In the LS model, the equation of motion for a target (projectile) of the areal mass density $\sigma = \int_0^{l_t} \rho(l) dl$ (ρ is the mass density and l_t is the total thickness of the target), being accelerated by a radiation (photon) pressure of a laser pulse with the intensity $I(t)$ may be conveniently written in the form:^{24,37}

$$\frac{\gamma}{1 - \beta} \frac{d\beta}{dw} = \frac{2I(w/c)}{\sigma c^3},$$

where $\beta = v/c$, $\gamma = (1 - \beta^2)^{-1/2}$, $w = ct - x$ is the retarded time variable, and we assumed for simplicity that the reflection coefficient for the target $R_t = 1$ (it is a fairly good approximation for circularly polarized laser pulses as in such a case a heating of the target by the pulse is small). To generalize this model to the LICPA scheme, we have to incorporate the effect of reflections inside the cavity. Let us denote by w_j the values of w for which the laser pulse reflected from the target strikes the cavity wall at the origin of the coordinate system for the j th time. We may then define a sequence of functions $x^{(j)}(w)$ with $j = 1, 2, \dots$, representing the position of the target for w in the interval $[w_{j-1}, w_j]$, and a sequence of functions $e^{(j)}(w)$ representing the total laser energy incident on the target, expressed in units of half of the relativistic rest energy of the foil. We assume $w_0 = 0$, $x^{(1)}(0) = L_c$; then $w_1 = 2L_c$, and more generally $w_{j+1} = w_j + 2x^{(j)}(w_j)$. Given

$e^{(j)}(w)$, the relativistic projectile velocity is then given by $\beta^{(j)}(w) = [(1 + e^{(j)}(w))^2 - 1] / [(1 + e^{(j)}(w))^2 + 1]$, and $x^{(j)}(w)$ may be determined by integrating the equation $dx/dw = \beta / (1 - \beta)$. We then have

$$e^{(j+1)}(w) = e^{(j)}(w_j) + \frac{2}{\sigma c^3} \int_{w_j}^w I(w'/c) dw' + R_c \frac{e^{(j)}(w^{(j)}(w)) - e^{(j)}(w_{j-1})}{(1 + e^{(j)}(w^{(j)}(w)))(1 + e^{(j)}(w_{j-1}))},$$

where R_c represents the reflection coefficient from the inner cavity wall. The function $w^{(j)}(w)$ gives the value of the retarded time from the interval $[w_{j-1}, w_j]$ characterizing the ray, which after reflection from the accelerated target strikes the inner cavity wall at the instant w belonging to the interval $[w_j, w_{j+1}]$. This set of formulas allows us to determine the position and the kinetic energy E_p of the projectile in a recursive way (or the kinetic energy fluence $F_p = E_p/S$ when the projectile area S is not defined). Knowing E_p (or F_p), we may then to determine the mean ion energy $\langle E \rangle$, provided that the ion number (or density) in the projectile is known. Thus, the model provides values of the projectile parameters (e.g., velocity, energy fluence, mean ion energy, and acceleration efficiency) as a function of the acceleration length, which could be compared with the corresponding values from the PIC simulations.

The PIC simulations revealed that the LICPA accelerator produces a compact, near-solid density, quasi-neutral plasma projectile (Fig. 10) with relatively narrow ion energy spectrum (Fig. 11), propagating with the subrelativistic velocity $v_p \sim 10^{10} \text{ cm/s}$. For a fixed value of the areal mass density σ of the projectile, the values of the mean ion energy per amu $\langle E \rangle/A$, the kinetic energy fluence F_p , and, as a result, the acceleration efficiency $\eta_{\text{acc}} = E_p/E_L = F_p/F_L$ (F_L is the laser energy fluence) are almost independent of the kind of ions, which form the projectile (Fig. 12). The acceleration

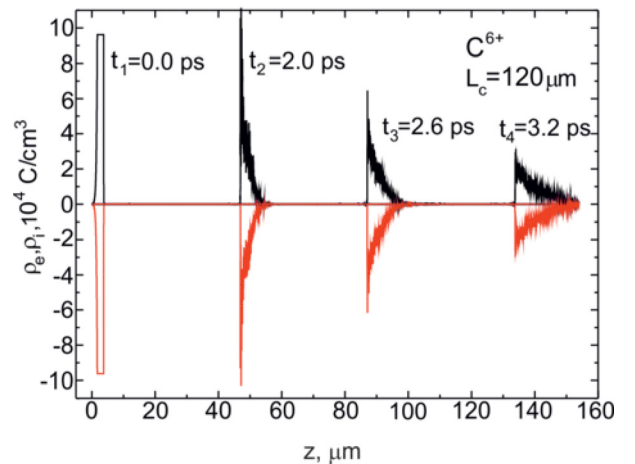


FIG. 10. Snapshots of the space distributions of the ion charge ρ_i and the electron charge ρ_e for the carbon plasma projectile accelerated in the photon pressure-driven LICPA accelerator of $L_c = 120 \mu\text{m}$ and $R_c = 0.64$. $I_L = 2.5 \times 10^{21} \text{ W/cm}^2$, $\tau_L = 2 \text{ ps}$, $\lambda = 1.06 \mu\text{m}$, $L_T = 2 \mu\text{m}$, $n_e = 6n_i = 6 \times 10^{23} \text{ cm}^{-3}$.

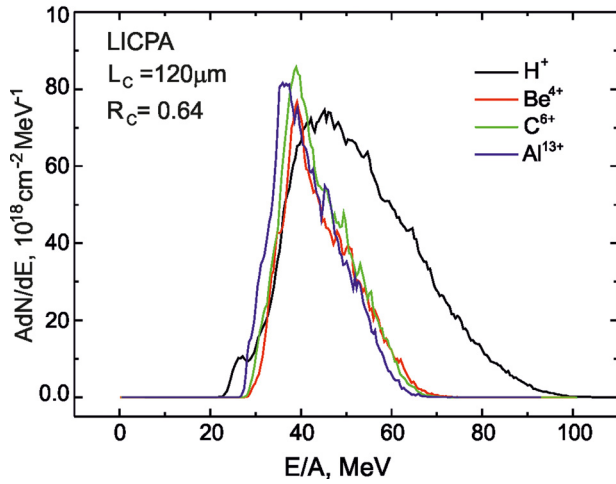


FIG. 11. The ion energy spectra of plasma projectiles of various kinds of ions accelerated in the photon pressure-driven LICPA accelerator. For all kinds of ions, $\sigma_h = \rho L_T = 4 \times 10^{-4} \text{ g/cm}^2$ and $L_T(\text{Al}^{13+}) = 1.48 \text{ } \mu\text{m}$, $L_T(\text{C}^{6+}) = 2 \text{ } \mu\text{m}$, $L_T(\text{Be}^{4+}) = 2.16 \text{ } \mu\text{m}$, $L_T(\text{H}^+) = 28.6 \text{ } \mu\text{m}$. Parameters of the LICPA accelerator and the laser driver are the same as in Fig. 10.

efficiency in the LICPA scheme reaches values in excess of 40%, which are by a factor of 2 higher than efficiencies obtained for the radiation pressure acceleration without the cavity enhancement, despite rather conservative assumption on the reflection coefficient inside the cavity $R_c = 0.64$.

The predicted parameters of the plasma projectile (which can also be treated as an ion beam) are extremely high, and for the LICPA-driven projectile (ion beam), they are as follows: the ion beam energy fluence $F_p \approx 2 \text{ GJ/cm}^2$, the peak beam intensity $I_p \sim 10^{22} \text{ W/cm}^2$, the peak ion current density $j_p \sim 10^{14} \text{ A/cm}^2$, the ion pulse duration $\tau_p < 1 \text{ ps}$. As a matter of comparison, I_p is by 2 orders and j_p by 7 orders of magnitude higher than those produced by Large Hadron Collider, although the ion energies are here lower by $\sim 4\text{--}5$ orders of magnitude. At the laser energy $E_L = 100 \text{ kJ}$, the projectile (ion beam) energy reaches $E_p \approx 40 \text{ kJ}$. If we also take into account the fact that the ion energy spectra are fairly well matched to the need of optimal stopping power in the

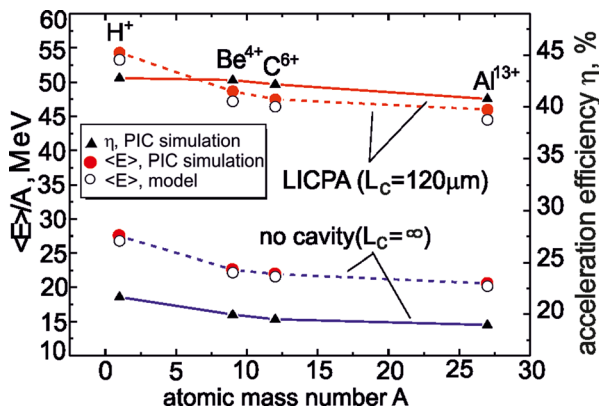


FIG. 12. The acceleration efficiency and the mean ion energy per amu of plasma projectiles of various kinds of ions driven in the LICPA accelerator or in the conventional RPA scheme (no cavity) as predicted by PIC simulations and the generalized LS model. Parameters of the LICPA accelerator, the laser driver, and the target are the same as in Figs. 10 and 11. The acceleration length is $l_{\text{acc}} = 200 \text{ } \mu\text{m}$.

compressed DT fuel (at least for Be^{4+} , C^{6+} , and Al^{13+}),⁴² we find that the plasma projectile (ion beam) produced in the LICPA accelerator meets very well the requirements for the ICF ion fast ignition.^{41–43}

Fig. 12 also demonstrates good agreement between the results obtained from the PIC simulations and those predicted by the generalized LS model. Relying on the consistency of these predictions, we may estimate the performance of the radiation pressure-driven LICPA accelerator for other values of the laser parameters. In particular, we have found that η_{acc} increases with the ratio $2F_L/\sigma c^2 = e$, and for $e \geq 0.5$, it is possible to reach $\eta_{\text{acc}} \approx 60\text{--}70\%$ even at a conservative assumption on the cavity parameters (e.g., $R_c = 0.64$, $L_c = 120 \text{ } \mu\text{m}$). Moreover, the ratio $R_{\eta}' = \eta_{\text{acc}}^{\text{LICPA}}/\eta_{\text{acc}}^{\text{RPA}}$ is increasing with increasing σ , which means that the LICPA accelerator can be especially useful for acceleration to very high ($\gg 10^8 \text{ cm/s}$) velocities of heavy projectiles, which is of particular interest for HEDP and ICF research.

V. CONCLUSIONS

The measurements performed using various diagnostics, combined with 2-dimensional hydrodynamic simulations have proven that the hydrodynamic LICPA accelerator can produce fast ($v_p > 10^7 \text{ cm/s}$) and dense plasma projectiles with the energetic efficiency of higher by an order of magnitude compared to the AA. The efficiency of the hydrodynamic accelerator weakly depends on the laser wavelength (contrary to AA), and both for the long-wavelength (NIR) and the short-wavelength (VIS, UV) laser beams, it can reach values in excess of 50%.

The PIC simulations and the generalized LS model have demonstrated that the photon pressure-driven LICPA accelerator can be a highly efficient scheme for acceleration of dense plasma projectiles up to near-relativistic velocities and, in particular, it can produce ultraintense, quasisimonoenergetic ion bunches of multi-MeV to multi-GeV ion energy with the energetic efficiency approaching 50%.

The LICPA accelerator may be in principle driven by laser beams covering a broad range of pulse energies, laser intensities, and pulse lengths, as well as laser wavelengths and repetition rates. As a result, the accelerator can produce dense, fast, and ultrafast projectiles of a wide variety of parameters, which creates a prospect for a broad range of the accelerator applications, particularly in such domains as ICF research (ion fast ignition, impact ignition), HEDP, nuclear physics, medicine (e.g., production of radioisotopes for PET), or pharmacology (e.g., precise drug injection by a LICPA-driven biolistic gun^{43,44}).

ACKNOWLEDGMENTS

We acknowledge the expert support of M. Pfeifer, P. Pisarczyk, J. Skala, and the PALS laser team as well as useful discussion with J. Wołowski and Yong-Joo Rhee. This work was supported in part by the Ministry of Science and Higher Education (MNiSZW), Poland under Grant No N202 207438, the Czech Ministry of Education, projects MSM6840770022, MSM6840770010, LC528, and the Czech Science Foundation,

Grant No. P201/10/P086. The experiment was performed within the Access to Research Infrastructure activity in the Seventh Framework Programme of the EU (Contract No 212025, Laserlab Europe-Continuation).

- ¹R. P. Drake, *High-Energy-Density Physics* (Springer, Berlin, 2006).
- ²A. Atzeni and J. Meyer-ter-Vehn, *The Physics of Inertial Fusion* (Clarendon, Oxford, 2004).
- ³K. W. D. Ledingham and W. Galster, *New J. Phys.* **12**, 045005 (2010).
- ⁴J. F. Friichtenicht and D. G. Becker, *Astrophys. J.* **166**, 717 (1971).
- ⁵T. F. Thornhill, L. C. Chhabildas, W. D. Reinhart, and D. L. Davidson, *Int. J. Impact Eng.* **33**, 799 (2006).
- ⁶T. R. Wolfe, P. Riedy, and D. Lewis, *IEEE Trans. Magn.* **37**, 506 (2001).
- ⁷R. W. Lemke, M. D. Knudson, and J.-P. Davis, *Int. J. Impact Eng.* **38**, 480 (2011).
- ⁸J. H. Degnan, R. E. Peterkin, Jr., G. P. Baca, J. D. Beason, D. E. Bell, M. E. Dearborn, D. Dietz, M. R. Douglas, S. E. Englert, T. J. Englert, K. E. Hackett, J. H. Holmes, T. W. Hussey, G. F. Kiuttu, F. M. Lehr, G. J. Marklin, B. W. Mullins, D. W. Price, N. F. Roderick, E. L. Ruden, C. R. Sovinec, and P. J. Turchi, *Phys. Fluids B* **5**, 2938 (1993).
- ⁹M. Murakami, H. Nagatomo, T. Sakaiya, H. Azechi, S. Fujioka, H. Gardner, J. Bats, D. Colombant, J. Weaver, and Y. Aglitskiy, *Plasma Phys. Controlled Fusion* **47**, B815 (2005).
- ¹⁰M. Karasik, J. L. Weaver, Y. Aglitskiy, T. Watatri, Y. Arikawa, T. Sakaiya, J. Oh, A. L. Velikovich, S. T. Zalesak, J. W. Bates, S. P. Obenschain, A. J. Schmitt, M. Murakami, and H. Azechi, *Phys. Plasmas* **17**, 056317 (2010).
- ¹¹A. Macchi, F. Cattani, T. V. Liseykina, and F. Cornalti, *Phys. Rev. Lett.* **94**, 165003 (2005).
- ¹²W. Yu, H. Xu, F. He, M. Y. Yu, S. Ishiguro, J. Zhang, and A. Y. Wong, *Phys. Rev. E* **72**, 046401 (2005).
- ¹³J. Badziak and S. Jabłoński, *Appl. Phys. Lett.* **99**, 071502 (2011).
- ¹⁴S. H. Glenzer, B. J. MacGowan, P. Michel, N. B. Meezan, L. J. Suter, S. N. Dixit, J. L. Kline, G. A. Kyrala, D. K. Bradley, D. A. Callahan, E. L. Dewald, L. Divol, E. Dzenitis, M. J. Edwards, A. V. Hamza, C. A. Haynam, D. E. Hinkel, D. H. Kalantar, J. D. Kilkenny, O. L. Landen, J. D. Lindl, S. LePape, J. D. Moody, A. Nikroo, T. Parham, M. B. Schneider, R. P. J. Town, P. Wegner, K. Widmann, P. Whitman, B. K. F. Young, B. Van Wonterghem, L. J. Atherton, and E. I. Moses, *Science* **327**, 1228 (2010).
- ¹⁵M. Murakami, H. Nagatomo, H. Azechi, F. Ogando, M. Perlado, and S. Eliezer, *Nucl. Fusion* **46**, 99 (2006).
- ¹⁶H. Azechi, T. Sakaiya, T. Watari, M. Karasik, H. Saito, K. Takeda, H. Hosoda, H. Shiraga, M. Nakai, K. Shigemori, S. Fujioka, M. Murakami, H. Nagatomo, T. Johzaki, J. Gardner, D. G. Colombant, J. W. Betes, A. L. Velikovich, Y. Aglitskiy, J. Weaver, S. Obenschain, S. Eliezer, R. Kodama, T. Norimatsu, H. Fujita, K. Mima, and H. Kan, *Phys. Rev. Lett.* **102**, 235002 (2009).
- ¹⁷H. Azechi, N. Miyanaga, S. Sakabe, T. Yamanaka, and C. Yamanaka, *Jpn. J. Appl. Phys.* **20**, L477 (1981).
- ¹⁸S. Borodziuk, A. Kasperczuk, T. Pisarczyk, J. Ullschmied, E. Krousky, K. Masek, M. Pfeifer, K. Rohlena, J. Skala, and P. Pisarczyk, *Appl. Phys. Lett.* **93**, 101502 (2008).
- ¹⁹J. Badziak, K. Kasperczuk, P. Parys, T. Pisarczyk, M. Rosiński, L. Ryć, J. Wołowski, R. Suchańska, J. Krasa, E. Krousky, L. Laska, K. Masek, M. Pfeifer, K. Rohlena, J. Skala, J. Ullschmied, I. B. Foldes, T. Suta, A. Borrielli, A. Mezzasalma, L. Torrissi, and P. Pisarczyk, *Appl. Phys. Lett.* **92**, 211502 (2008).
- ²⁰K. Otani, K. Shigemori, T. Sakaiya, S. Fujioka, A. Sunahara, M. Nakai, H. Shiraga, H. Azechi, and K. Mima, *Phys. Plasmas*, **14**, 122702 (2007).
- ²¹T. Esirkepov, M. Borghesi, S. V. Bulanov, G. Mourou, and T. Tajima, *Phys. Rev. Lett.* **92**, 175003 (2004).
- ²²A. P. L. Robinson, M. Zepf, S. Kar, R. G. Evans, and C. Bellei, *New J. Phys.* **10**, 033034 (2008).
- ²³T. V. Liseykina, M. Borghesi, A. Macchi and S. Tuveri, *Plasma Phys. Controlled Fusion* **50**, 124033 (2008).
- ²⁴A. Macchi, S. Veghini, and F. Pegoraro, *Phys. Rev. Lett.* **103**, 085003 (2009).
- ²⁵J. Badziak, S. Jabłoński, and S. Głowacz, *Appl. Phys. Lett.* **89**, 061504 (2006).
- ²⁶J. Badziak, S. Jabłoński, P. Parys, M. Rosiński, J. Wołowski, A. Szydłowski, P. Antici, J. Fuchs, and A. Mancic, *J. Appl. Phys.* **104**, 063310 (2008).
- ²⁷J. Badziak, S. Borodziuk, T. Pisarczyk, T. Chodukowski, E. Krousky, K. Masek, J. Skala, J. Ullschmied, and Y.-J. Rhee, *Appl. Phys. Lett.* **96**, 251502 (2010).
- ²⁸K. Jungwirth, A. Cejnarova, L. Juha, B. Kralikova, J. Krasa, E. Krousky, P. Krupickova, L. Laska, K. Masek, A. Prag, O. Renner, K. Rohlena, B. Rus, J. Skala, P. Straka, and J. Ullschmied, *Phys. Plasmas* **8**, 2495 (2001).
- ²⁹A. Kasperczuk and T. Pisarczyk, *Opt. Appl.* **31**, 571 (2001).
- ³⁰E. Woryna, W. Mróz, P. Parys, and J. Wołowski, *Laser Part. Beams* **14**, 293 (1996).
- ³¹R. Liska, M. Kucharik, J. Limpouch, O. Renner, P. Vachal, L. Bednarik, J. Velechovsky, in *Finite Volumes for Complex Applications VI, Problems & Perspectives*, edited by J. Fort, J. Furst, J. Halama, R. Herbin, and F. Hubert (Springer-Verlag, 2011), Vol. 2, pp. 57–73.
- ³²C. Hirt, A. Amsden, and J. Cook, *J. Comput. Phys.* **14**, 227 (1974). Reprinted in **135**, 203 (1997).
- ³³E. J. Caramana, D. E. Burton, M. J. Shashkov, and P. P. Whalen, *J. Comput. Phys.* **146**, 227 (1998).
- ³⁴M. Kucharik, M. Shashkov, and B. Wendroff, *J. Comput. Phys.* **188**, 462 (2003).
- ³⁵M. Shashkov and S. Steinberg, *J. Comput. Phys.* **129**, 383 (1996).
- ³⁶T. Kapin, M. Kucharik, J. Limpouch, R. Liska, and P. Vachal, *Int. J. Numer. Methods Fluids* **56**, 1337 (2008).
- ³⁷G. Marx, *Nature (London)* **211**, 22 (1966).
- ³⁸J. Badziak and S. Jabłoński, *Phys. Plasmas* **17**, 073106 (2010).
- ³⁹R. Lichters, R. E. W. Pfund and J. Meyer-ter-Vehn, LPIC++: A parallel one-dimensional relativistic electromagnetic particle-in-cell-code for simulating laser-plasma-interactions. Report No. MPQ 225, Max-Planck Institut fur Quantenoptik Garching, Germany (1997), the code is available at <http://www.lichters.net/download.html>
- ⁴⁰J. C. Fernandez, J. J. Honrubia, B. J. Albright, K. A. Flippo, D. Cort Gautier, B. M. Hegelich, M. J. Schmitt, M. Temporal, and L. Yin, *Nucl. Fusion* **49**, 065004 (2009).
- ⁴¹J. Davis, G. M. Petrov, and T. A. Mehlhorn, *Plasma Phys. Controlled Fusion* **53**, 045013 (2011).
- ⁴²J. J. Honrubia, J. C. Fernandez, M. Temporal, B. M. Hegelich, and J. Meyer-ter-Vehn, *Phys. Plasmas* **16**, 102701 (2009).
- ⁴³V. Menezes, K. Takayama, A. Gojani, and S. H. R. Hasseini, *Shock Waves* **18**, 393 (2008).
- ⁴⁴T. Han, H. Lee, S. Choi, A. B. Gojani, and J. J. Yoh, *Appl. Phys. A* **101**, 417 (2010).